

LA-UR-19-31213 (Accepted Manuscript)

Shear strength and permeability of the cement-casing interface

Welch, Nathan James
Frash, Luke Philip
Harp, Dylan Robert
Carey, James William

Provided by the author(s) and the Los Alamos National Laboratory (2020-10-26).

To be published in: International Journal of Greenhouse Gas Control

DOI to publisher's version: 10.1016/j.ijggc.2020.102977

Permalink to record: <http://permalink.lanl.gov/object/view?what=info:lanl-repo/lareport/LA-UR-19-31213>

Disclaimer:

Los Alamos National Laboratory, an affirmative action/equal opportunity employer, is operated by Triad National Security, LLC for the National Nuclear Security Administration of U.S. Department of Energy under contract 89233218CNA000001. By approving this article, the publisher recognizes that the U.S. Government retains nonexclusive, royalty-free license to publish or reproduce the published form of this contribution, or to allow others to do so, for U.S. Government purposes. Los Alamos National Laboratory requests that the publisher identify this article as work performed under the auspices of the U.S. Department of Energy. Los Alamos National Laboratory strongly supports academic freedom and a researcher's right to publish; as an institution, however, the Laboratory does not endorse the viewpoint of a publication or guarantee its technical correctness.

Shear strength and permeability of the cement-casing interface

N.J. Welch^{a*}, L.P. Frash^a, D.H. Harp^a and J.W. Carey^a

^aEarth and Environmental Sciences Division, Los Alamos National Laboratory, Los Alamos, NM 87545, USA

*Corresponding Author: nwelch@lanl.gov; Los Alamos National Laboratory, P.O. Box 1663, MS D462, Los Alamos, NM 87454

Abstract

The shear strength and hydraulic permeability of the interface between well cement and casing was investigated using a triaxial direct shear apparatus. For the first time, these experiments provide measurements under controlled stress conditions with fluid flow measurements along the interface. The low cohesion (1.1 ± 1.1 MPa) and the high friction angle ($43.4 \pm 2.0^\circ$) indicates that the shear strength of the interface is provided by friction. This implies that the state of stress of the cement is critical to well integrity. The hydraulic aperture of the undamaged cement-steel samples was 6.8 ± 1.0 microns. Shear damage to the interface caused a decrease (-20%) in hydraulic aperture for samples aged up to 1 month, and an increase (+300%) for samples cured for two years. We performed numerical simulations to estimate the leakage potential from a carbon storage operation. This model predicts negligible leakage amounts (47 tonnes) in a shear-damaged well for the modeled injection of ~ 1.26 million tonnes of CO_2 . Thus, our measurements indicate that the cement-casing interface is not a significant leakage pathway in its intact or damaged state, and that shear-driven failure scenarios for this interface are not a significant risk to CO_2 storage security.

Keywords

Well Integrity; Well Leakage; Geologic Carbon Storage; Shear Damage, Zonal Isolation

1. Introduction

The well seal provided by cement is essential in minimizing interzonal and surface migration of fluids around a well casing in subsurface hydrocarbon and carbon sequestration reservoirs (Carey, 2013; Carroll et al., 2016; Crow et al., 2010; Zhang and Bachu, 2011). Of particular importance is protection of shallow aquifers from oil and gas contamination (Dahi Taleghani and Wang, 2016) and the long-term safe storage requirements of carbon dioxide needed for conformance to EPA guidelines (Benson and Cook, 2005; U.S. E.P.A., 2012). Well leakage

22 and failure can be caused by faulty cementing or abandonment, formation damage, mud channeling, gas
23 migration during curing, and stress-induced failure (Carey, 2013; Zhang and Bachu, 2011). The interfaces
24 between 1) casing and cement and 2) cement and formation have been identified as preferential pathways for
25 fluid leakage in wells (Carey et al., 2007; Dusseault et al., 2000). Wells drilled and plugged and abandoned with
26 no casing have been found to have a significantly lower risk of leakage than wells with casing present (Watson
27 and Bachu, 2009). It is therefore critical to understand the processes that control leakage at the cement-casing
28 interface for continued improvement of well design.

29 In this study, we focus on shear-induced mechanical damage to the cement-steel interface that could lead to
30 leakage. The key parameters of interest are the shear and normal stresses at the interface, the strength of the
31 steel-cement bond, and the frictional properties of the cement-steel interface. Experimental investigation of the
32 shear strength of the well casing and cement interface strength began in the early 1960s with the “pushout”
33 laboratory test of Carter and Evans (Carter and Evans, 1964; Evans and Carter, 1962). In this technique cement
34 is cured in the annulus between a containing steel ring and a central steel casing. The steel casing is then driven
35 out of the cement sheath while measuring the force required to shear the interface. This experimental method
36 has been used in a number of other works to investigate variables impacting the shear strength of the cement-
37 steel interface (Carpenter et al., 1992; Hwang et al., 2018; Kakumoto et al., 2012; Lavrov et al., 2019; Parcevaux
38 and Sault, 1984; Silva Neto et al., 2014). In addition, several other approaches have been used to characterize
39 the cement-steel bond strength including the slant-shear method in which cement is cast against a steel cylinder
40 with a 60° slanted surface and strength is measured by compressing the assembly (Genedy et al., 2014; Liu et
41 al., 2015); a classical friction sliding experiment in which the stress to move a block of cement across a steel
42 plate is measured as a function of the normal stress (Rabbat and Russell, 1985); and a pushout-type of
43 experiment conducted in a triaxial cell (Kakumoto et al., 2012).

44 In order to understand potential leakage in the subsurface, experimental data are needed to develop models of
45 shear damage and the hydraulic conductivity of shear-damaged interfaces. Understanding mechanical damage
46 to the cement-steel interface requires shear-stress measurements as a function of normal stress to the interface
47 to develop a failure model such as the Mohr-Coulomb criterion. Because the traditional pushout and the slant-
48 shear tests are conducted at a single condition, they cannot provide the cohesion and friction properties needed
49 for a model such as Mohr-Coulomb. A recent investigation of the traditional pushout test has shown a strong

50 dependence of shear-strength on experimental geometry, possibly due to cement shrinkage and the
51 unconstrained normal stress at the interface (Lavrov et al., 2019). Of the studies described above, only the work
52 of Kakumoto et al. (2012) is suitable for extracting the needed mechanical parameters for the cement-steel
53 interface. The classical friction-sliding method satisfies the requirements, but data are only available on concrete
54 sliding against steel (Rabbat and Russell, 1985). None of these studies address the question of how shear
55 damage modifies the hydraulic conductivity of the interface.

56 The cement-steel interface can also be damaged by tensile opening of cement and casing interface due to
57 injection fluid pressure greater than the normal stress. This increase could arise during carbon dioxide
58 sequestration operations and hydraulic stimulation operations. Theoretical (Frash and Carey, 2018; Lecampion
59 et al., 2013), experimental (Lecampion et al., 2013), and numerical (Feng et al., 2017) analyses of the tensile
60 opening of a bonded annulus driven by fluid injection have also been completed. Although not directly addressed
61 in our experimental investigation, the bond strengths that we derive apply to tensile failure as well as to fluid
62 injection-induced shear failure.

63 The need for a complete understanding of the mechanical and hydrological properties of the cement-steel
64 interface are highlighted by theoretical and computational studies (Bois et al., 2011; Feng et al., 2017; Frash and
65 Carey, 2018; Lecampion et al., 2013). In all of these studies, the properties of the interface had to be assumed.
66 For example, the recent theoretical analysis of (Frash and Carey, 2018) developed a tool for analyzing cement-
67 casing shear damage, including the mechanical behavior of the casing, cement, and formation, fluid flow through
68 the porous media, and the character of the bonding interface. However, this work had to assume values for the
69 strength and frictional properties of the cement-casing interface, which were shown to have a significant impact
70 on model results. A new method for obtaining these properties while also yielding interface permeability data
71 would be beneficial in better constraining model input parameters leading to improved ability to analyze wellbore
72 integrity.

73 In this work, we obtained strength and permeability data for the cement-casing bond under varying stress
74 conditions analogous to the depth of a wellbore using an experimental system with well-defined stress boundary
75 conditions. We used the triaxial direct-shear method in which bonded, half-cylinders of steel and cement are
76 sheared while a constant normal stress is applied across the cement-steel interface (Carey et al., 2015; Frash
77 et al., 2017). By performing measurements as a function of confining stress and displacement, we obtained the

78 intact and de-bonded cohesion and frictional properties of the cement-casing interface. The triaxial direct shear
79 system also provided continuous measurement of fluid flow across the length of the cement-casing interface
80 allowing full characterization of the hydraulic properties before and after shearing. Our results quantify the initial
81 permeability of the cured cement-casing interface along with changes caused by shear damage of the sample.
82 From these measurements we find that cement-steel intact cohesion is small to negligible 1.1 ± 1.1 MPa and the
83 friction angle is relatively high $43.4 \pm 2.0^\circ$. Therefore, interface strength is controlled primarily by friction and
84 confining stress and not the strength of the bond.

85 Experimental characterization of the permeability of the interface showed non-zero but relatively small values
86 equivalent to a hydraulic aperture of 6.8 ± 1.0 microns prior to shearing and that shear displacement only weakly
87 modified the interface permeability. We evaluated the significance of the measured permeability by performing
88 numerical simulations of a leaking well at a model CO₂ sequestration injection site. The results showed that
89 despite the finite permeability of the casing-cement interface, the quantity of CO₂ escaping was negligible during
90 a 20-year period (less than 50 tonnes in a 1.3 Mt injection project).

91 2. Methods

92 Experiments were conducted using a triaxial direct shear apparatus (Carey et al., 2015; Frash et al., 2017, 2016)
93 using composite cement-steel specimens. Figure 1 provides a diagram of the direct-shear coreholder assembly
94 and images of the cement-steel sample preparation. The steel and cement samples were prepared using 1-inch
95 diameter, thin plastic tubing as a support for poured cement on the opposing face of steel half-rounds (Figure
96 1b). The steel half-rounds had a 1 inch diameter and were 1 inch in length with a black mill varnish typical of well
97 casings to prevent corrosion on the flat surface bonded to the cement. The cement used was Ash Grove oil well
98 cement type G and was prepared in small batches according to ASTM C305, mixing by hand with a water-to-
99 cement mass ratio of 0.4. Prior to mixing, the dry cement mix was passed through a No. 35 sieve to disaggregate
100 clumps. Following mixing, the cement was poured into the tubing containing three steel half-rounds separated
101 by thin, cured cement half-rounds to aid in later separation.

102 Samples were allowed to cure in three time intervals of 1 week, 1 month, and 2 years to determine the effect of
103 cure time on measured properties. These intervals were chosen to represent the initial performance of the
104 cement annulus immediately following completion, the beginning performance of a well, and the long-term

105 performance of a well. The 1 week and 1 month samples were allowed to cure at ambient temperature and
106 atmospheric pressure, upright prior to being sectioned. The 2 year samples were allowed to cure as individual
107 specimens at ambient temperature and atmospheric pressure until hard enough to be removed and submerged
108 in a calcium hydroxide solution for long term storage in a sealed container at ambient temperature and
109 atmospheric pressure. It should be noted that the curing conditions of cement can have significant impacts on
110 the mechanical properties of the cement during curing. The air cured specimens likely had significantly lower
111 compressive strength than the moist cured 2 year samples (Gonnerman and Shuman, 1928; Kosmatka et al.,
112 2002; Wood, 1992). The ends of the samples were ground square using a water-wetted polishing wheel. The
113 dimensions and mass of each sample were recorded.

114 An additional set of solid cement samples were prepared in a similar fashion with dimensions 2.5 x 2.5 cm
115 diameter and length, recovered from the upper, pure-cement section of the plastic tube columns shown in Figure
116 1. Experiments on the solid cement were completed after approximately one year of cure time.

117 Interface strength properties were measured with the triaxial direct shear system by applying force to opposing
118 halves of the axial faces of the cylindrical plug samples to induce shear along the cement-steel interface (Figure
119 1). The apparatus and methodology were originally developed for the study of shear behavior of rock systems
120 (Carey et al., 2015; Frash et al., 2017, 2016) but was readily modified by aligning the cement-steel interface with
121 the direct-shear plane. The direct shear stress applied to the samples was measured from the pressure applied
122 to the axial assembly of the cell by an ISCO syringe pump. The confining pressure of the system was controlled
123 by either gas regulator pressure or an ISCO syringe pump. The system allows for the measurement of fluid flow
124 rate through samples complemented by pressure transducer measurements on the inlet and outlet flow lines of
125 the cell. The displacement of the fractured specimens was measured by a linear variable differential transformer
126 (LVDT) affixed to the top of the axial assembly, and displacement was limited to 4 mm to avoid damage to the
127 confining sleeve. All system parameters were recorded and controlled through a National Instruments
128 workstation via the Los Alamos National Laboratory-developed Disco control software
129 (<https://www.lanl.gov/software/disco>).

130

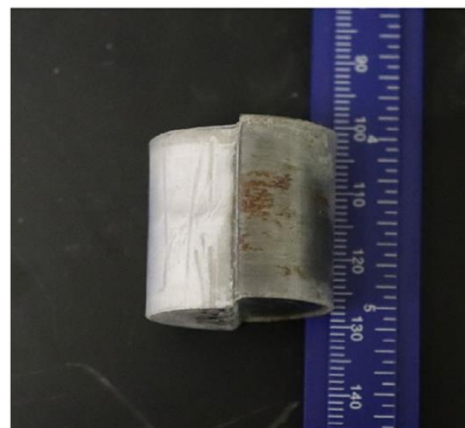
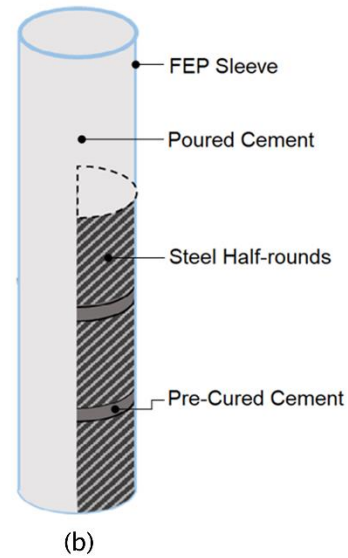
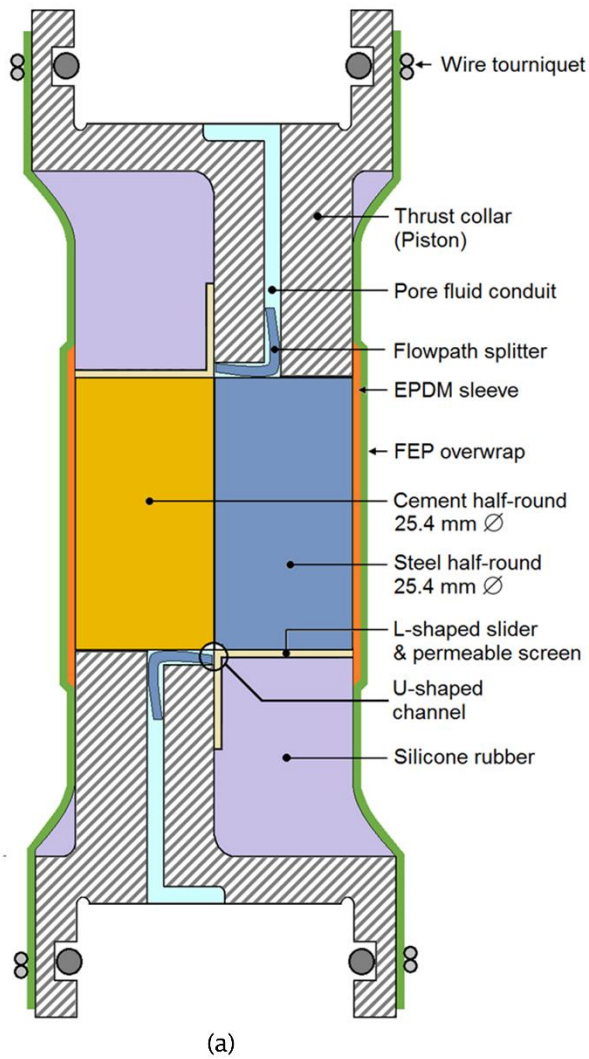


Figure 1: (a) Diagram of direct-shear collar assembly used in the triaxial direct-shear apparatus. (b) Diagram of the preparation of cement-steel half rounds with pre-cured cement half-rounds used to aid in later separation. (c) Image of post-experiment plug sample showing displaced cement-steel interface.

For the experiments, the cement-steel specimens were inserted into an ethylene propylene diene monomer (EPDM) rubber sleeve (Figure 1). A titanium direct-shear collar was inserted into each end of the EPDM sleeve aligning the shear edge with the interface of the cement-steel sample. Each collar assembly included silicone rubber which provided support for the EPDM sleeve and applied a deformable and approximately constant stress to the free end-surface of the specimen equal to the confining stress applied to the specimen circumference. An L-shaped metal shim was used to avoid extrusion of the rubber into the system pore space at high pressures (see (Frash et al., 2017) for details on the experimental direct-shear system). Each direct-shear collar has a pore fluid channel to provide pore fluid conductivity to the face of the specimen. The sample ends were topped with a thin metal mesh screen to provide pore fluid access to the entirety of the sample face. Finally, a fluorinated ethylene propylene (FEP) overwrap was heat shrunk to the entire assembly to isolate the sample from the

145 confining fluid and allow for the development of confining stress. Metal wires were wrapped around the base of
146 the thrust collars to provide mechanical stability and initial sealing of the FEP to the metal (Figure 1a).

147 The shear strength of the cement-steel interface was calculated from the direct-shear stress across the interface
148 (τ_{DS}) as (Frash et al., 2017):

$$149 \quad \tau_{DS} = \frac{F_P - F_C}{DL} - \sigma_s \quad (1)$$

150 Using the force applied by the piston (F_P) to a semi-circular area of the specimen, the force of the compression
151 of the rubber (F_C) applied to the other semi-circular half of the specimen originating from the confining fluid
152 pressure assuming a Poisson's ratio for silicone rubber of 0.5, the diameter of the sample (D), and the length of
153 the sample (L). The calibration term (σ_s) is a correction determined from system calibration that varies with shear
154 displacement. The magnitude of the uncertainty of this error term is shown as the error bars presented with each
155 individual measurement presented in the Results section below.

156 The effective confining stress (P_{eff}) was calculated using the Terzaghi effective stress relationship with a Biot
157 poroelastic term of 1.0, the average of the upstream (P_1) and downstream (P_2) pore pressures, and the confining
158 pressure (P_c) as:

$$159 \quad P_{eff} = P_c - 0.5(P_1 + P_2) \quad (2)$$

160 The hydraulic conductivity of the interface was characterized by the hydraulic aperture rather than permeability,
161 as the geometric area of flow at the interface is not well defined. The hydraulic aperture (b_H) of the samples was
162 calculated from the flow rate through the sample (Q), the viscosity of water ($\mu = 0.9$ cP), the width of the interface
163 ($w = 25.4$ mm), and the pressure gradient across the sample (∇P) using the cubic law equation for fluid flow
164 between parallel surfaces (Zimmerman and Bodvarsson, 1996):

$$165 \quad b_H = \sqrt[3]{-\frac{12Q\mu}{(\nabla P)w}} \quad (3)$$

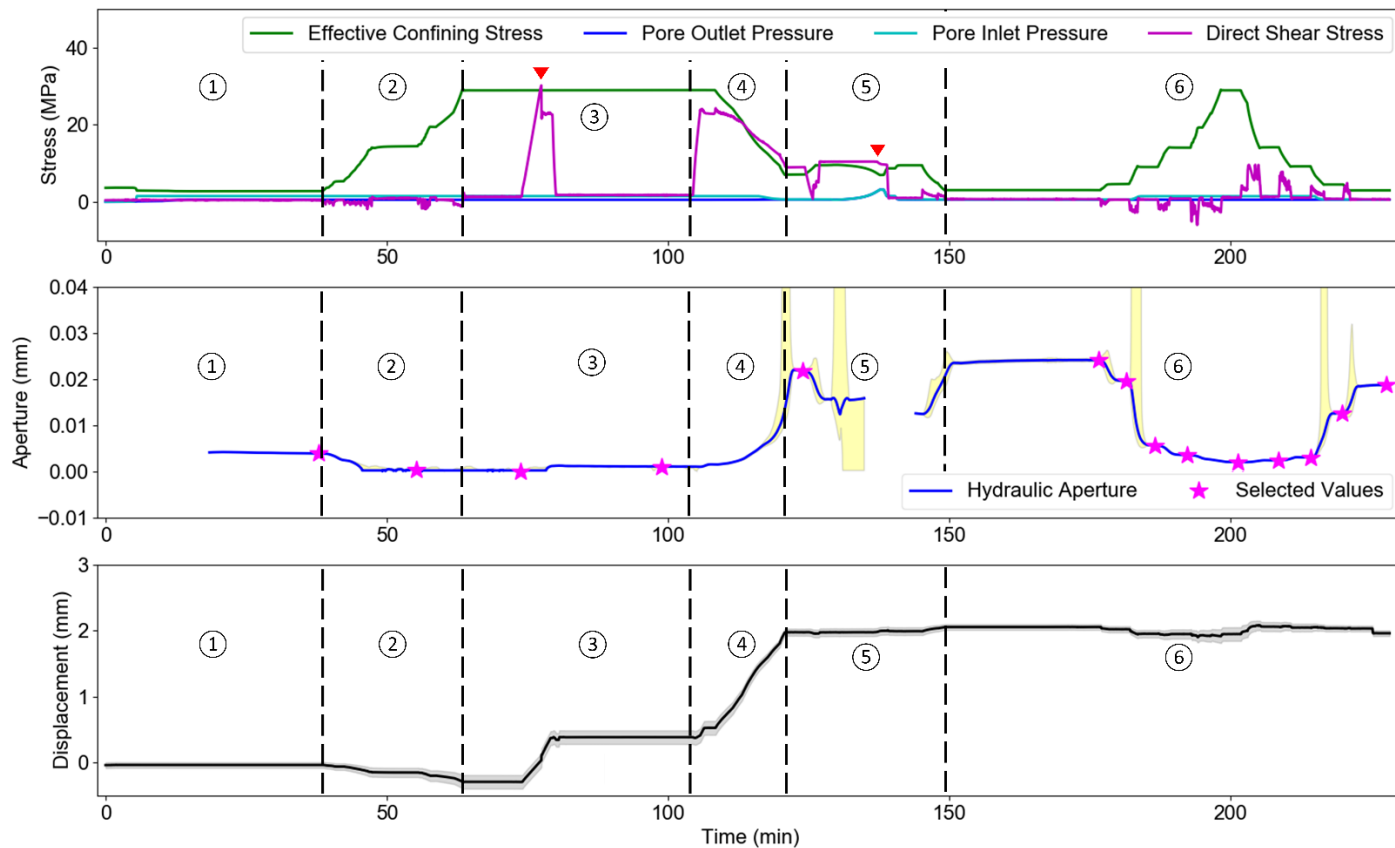
166

167 The triaxial direct shear tests were performed in a series of experimental steps as outlined in Figure 2. The
168 system was initialized with a small amount of direct shear stress to seat the sample and confining pressure was
169 raised to 3.5 MPa (①). The water in the pore lines of the system was pressurized to 0.5 MPa downstream
170 pressure and the upstream pump was operated at constant pressure of 1.5 MPa with a maximum flow rate of 1
171 ml/min. This control regime was employed to limit excessive flow rates for highly permeable samples and to
172 avoid rupture of the confining sleeve with low permeability samples. The system was allowed to stabilize for 15
173 minutes while measurement of the intact initial sample hydraulic aperture was collected at the same initial system
174 stresses for each sample. The confining pressure of the system was raised to the desired confining stress (if
175 greater than 3.5 MPa) for the intact shear strength measurement (②), and the system was again allowed to
176 stabilize and a pre-shear hydraulic aperture was measured. The intact shear-strength was measured by
177 increasing the direct shear stress at a constant rate until the sample failed, marked by a distinct drop in the
178 sustained direct shear stress supported by the sample (marked with a red arrow) and continuous displacement
179 (③). The direct shear stress was returned (③) to the low seating stress (creating approximately isostatic pressure
180 conditions) and a post-shear permeability was measured.

181 In the second stage of the experiment, the residual shear strength was measured in which the direct shear stress
182 was raised until displacement was reactivated. This test was done either as a single step or, as shown in Figure
183 2, as a dynamic measurement. In the latter case, the confining pressure was steadily lowered, reducing the
184 system effective confining stress, while maintaining the direct shear stress at a critical point to continuously
185 displace the sample under the changing stress conditions (④). This stage of the test provided a continuous
186 measurement of the residual shear strength of the interface as the effective confining stress was lowered. The
187 uncertainty in our fluid flow measurements during this stage increased substantially due to the fluid displacement
188 of the moving piston assembly.

189 In the third stage of the experiment, a hydroshear test was performed in which the downstream pump was
190 stopped while the upstream pump continued to flow resulting in increasing pore pressure in the fracture. The
191 direct shear stress was first raised to a value that the specimen was able to support without deformation at the
192 effective confining stress. The pore pressure of the fluid was raised at a slow rate, reducing the system effective
193 stress, until the system was again observed to displace and a drop in the supported direct shear stress was
194 observed (marked by a red arrow) (⑤). However, these results will not be presented in this work.

195 In the final stage of the experiment, a series of permeability measurements were performed as a function of
196 confining stress to determine the effect of normal stress on the hydraulic aperture of the interface. The confining
197 stress was raised and lowered in a step-wise fashion from 3.5 to 30 MPa and back again to observe the behavior
198 of the sheared interface with no further shear displacement ((6)).



199
200 Figure 2: Experiment stresses and pressures (top), hydraulic aperture (middle) with pink stars highlighting
201 stabilized measurement points, and displacement (bottom) for the two year sample CSS11-04. The numbered
202 regions show: (1) seating and establishment of confining and pore pressures; (2) raising confining pressure
203 for the intact shear strength measurement; (3) intact shear strength measurement by increasing direct shear
204 with the specimen failure point identified by the red arrow; (4) dynamic residual strength shear test, (5)
205 hydroshear test with the shear event marked with a red arrow; and (6) impact of changes in effective confining
206 stress on hydraulic fracture aperture. Yellow bands represent uncertainty in the hydraulic aperture measurement
207 that originate primarily from differing inlet/outlet flow rates.

208 Post-experiment profilometry and surface images were recorded using a VK-X150 shape measurement laser
209 microscope to determine the surface topography of the sheared cement. These results were used in quantifying
210 changes in surface roughness due to different cement curing times. Surface laser-optical images and
211 profilometry were collected with an image resolution of 10.91 μm and height resolution of 0.1 nm.

212 3. Results

213 In total, 19 samples were examined with intact shear strength and residual friction properties given in Table 1
214 and hydraulic properties given in Table 2. The initial hydraulic aperture was recorded at the end of a 15 minute
215 stabilization period and was taken at an effective normal stress of about 2.7 MPa for all samples. The effective
216 stress during shear is the confining stress used for the measurement of the intact shear strength. The post-shear
217 failure hydraulic aperture was recorded after returning the system to hydrostatic conditions corresponding to the
218 value given by the effective stress during shear. The hydraulic aperture of the solid cement samples was
219 calculated based on half of the flow to determine the contribution of flow coming from the cement matrix of the
220 cement-steel samples.

Table 1: Summary of the intact sample shear strength and post-shear residual friction.

Sample Group	Sample No.	Effective Confining Stress During Initial Shear (MPa)	Shear Stress of Initial Shear (MPa)	Residual Friction Angle (°)
1 Week	CSS12-01	2.7	1.8	36.0±0.7
	CSS12-02	2.6	2.1	41.0±1.0
	CSS12-03	2.7	3.6	41.0±0.9
	CSS13-01	28.9	20.4	46.9±0.2
	CSS13-02	9.1	7.3	41.0±1.0
	CSS13-03	29.0	17.9	42.7±1.0
1 Month	CSS10-01	3.0	2.9	33.6±0.6
	CSS10-02	2.9	3.3	34.3±2.9
	CSS10-03	29.3	26.7	35.5±3.8
	CSS14-01	9.0	10.5	40.7±1.3
	CSS14-02 ¹	-	-	-
	CSS14-03 ¹	-	-	-
2 Year	CSS11-01	3.1	4.8	28.0±1.4
	CSS11-02	2.8	3.5	33.7±0.5
	CSS11-03	2.7	2.1	34.4±1.6
	CSS11-04	28.9	28.3	36.3±0.4
Solid Cement	CEM01-01	9.5	19.9	51.6±0.5
	CEM01-02	2.8	7.9	51.0±1.0
	CEM01-03	28.0	36.4	56.4±0.9

¹Incomplete experimental results due to shear-collar impinging on steel.

Table 2: Summary of sample hydraulic conductivity expressed as hydraulic aperture (Eq. 3). Solid cement values have been adjusted to account for only half of the sample flow for comparison with the same flow area as the cement-steel samples.

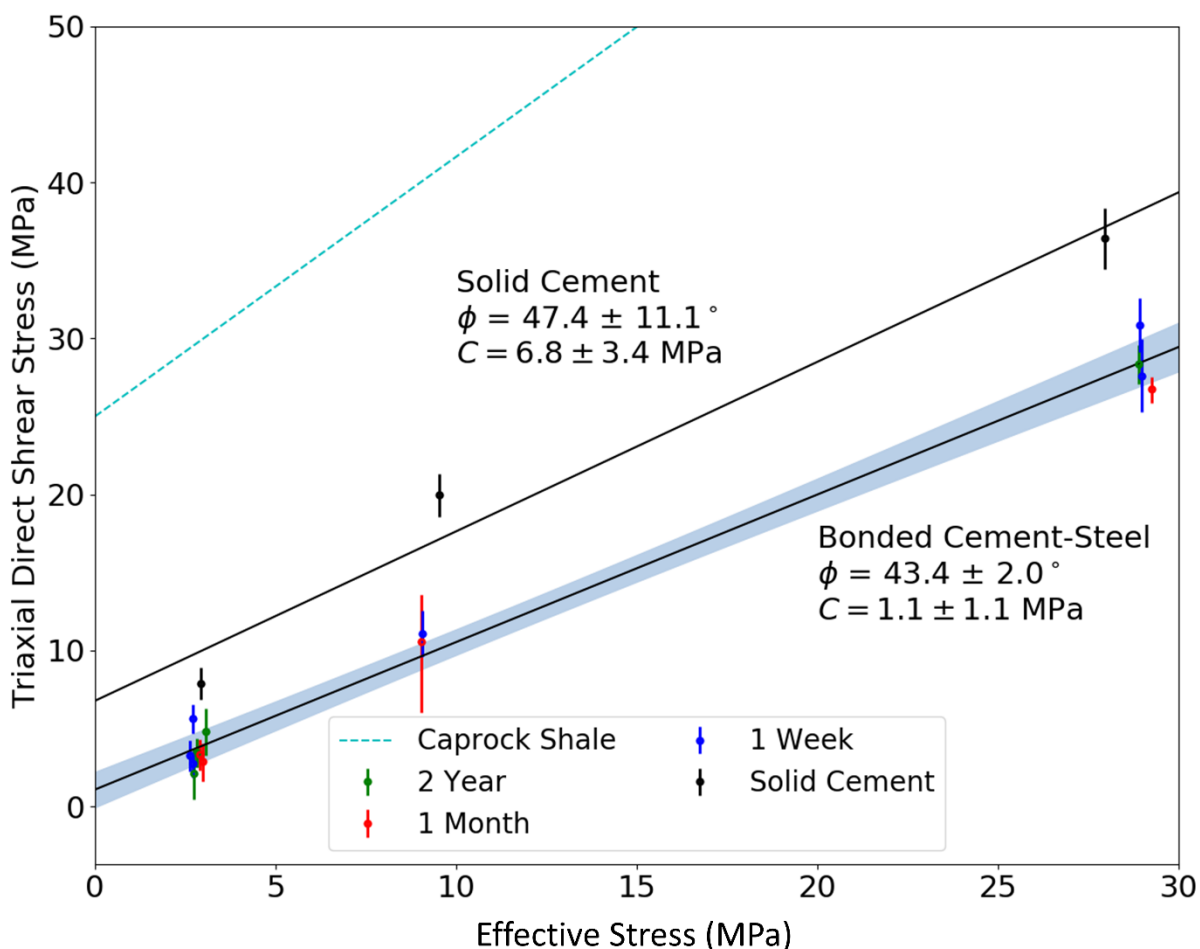
Sample Group	Sample No.	Initial Hydraulic Aperture (microns)	Effective Confining Stress during Shear (MPa)	Pre-shear Hydraulic Aperture (microns)	Post-shear Hydraulic Aperture (microns)
1 Week	CSS12-01	6.7	2.7	6.7	5.5
	CSS12-02	6.7	2.6	6.7	5.5
	CSS12-03	5.9	2.7	5.9	5.8
	CSS13-01 ¹	1.5	28.9	-	-
	CSS13-02	5.1	9.1	3.3	3.1
	CSS13-03	6.0	29.0	2.9	2.4
1 Month	CSS10-01	8.6	3.0	8.6	6.9
	CSS10-02	4.6	2.9	4.6	5.1
	CSS10-03	-	29.3	1.4	0.7
	CSS14-01	7.2	9.0	4.7	3.6
	CSS14-02 ²	7.4	-	-	-
	CSS14-03 ²	17.5	-	-	-
2 Year	CSS11-01	4.5	3.1	4.5	8.0
	CSS11-02	9.0	2.8	9.0	6.4
	CSS11-03	1.9	2.7	1.9	8.3
	CSS11-04	4.0	28.9	0.1	1.1
Solid Cement	CEM01-01	4.0	9.5	4.0	3.5
	CEM01-02	4.3	2.8	4.3	5.1
	CEM01-03	4.3	28.0	3.3	2.7

¹Fluid Flow port became blocked during experiment. ²Incomplete experimental results due to shear-collar impinging on steel.

3.1. Intact Shear Strength

The initial intact shear strength of each of the samples was investigated over a range of confining pressures from 3.5 MPa to 30 MPa (Table 1). The resulting data for the cement-steel interface samples and the solid cement are shown in Figure 3. A trend line was fit to each dataset representing the failure envelope with the shaded region showing the 95% confidence interval of the linear fit (Figure 3). Due to the lack of significant differences as a function of cure time, the cement-steel interface samples were fit with a single trend line. The intercept and

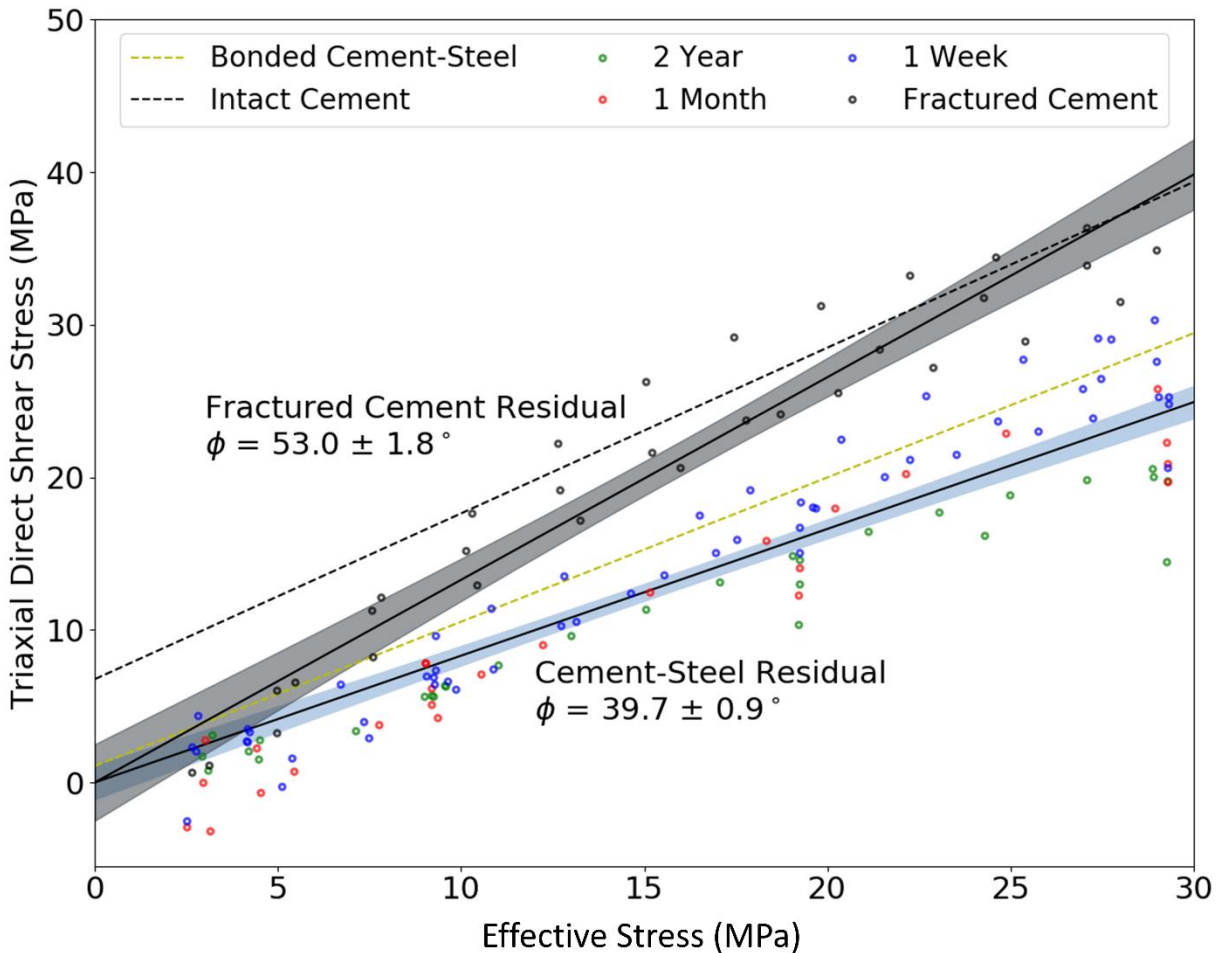
227 slope of the trendline were used to evaluate the cohesion (1.1 ± 1.1 MPa) and friction angle ($43.4 \pm 2.0^\circ$) in a
228 Mohr-Coulomb failure model.



229
230 Figure 3: Comparison of intact shear strengths for all samples as a function of effective normal stress including
231 linear fit and error band. The shear strength as measured using this equipment for Marcellus shale is included
232 as the dashed blue line for reference of caprock.

233 3.2. Residual Strength

234 The residual strength of the cement steel interface after shearing was measured for each of the samples in
235 individual shear steps or by using a dynamic method. As the dynamic technique results in a continuous
236 measurement of the residual shear strength of the interface, 10 points were selected along the length of the test
237 to be plotted along with the stepwise measurements. A linear fit of the data was used to determine the Mohr-
238 Coulomb failure envelope and 95% confidence interval of the linear fit is shown as a shaded region (Figure 4).
239 The cohesion was considered to be zero as the samples had already been sheared. Included in this figure are
240 the initial cement and bonded cement-steel shear strength failure envelope shown as dashed lines for ease of
241 comparison.



242
243
244
245
246

Figure 4: Residual shear strength of the cement-steel interface and the fractured cement showing data points, fitted line, and 95% confidence intervals (cement-steel fit shown with blue confidence and fractured cement in gray). For reference, the dashed yellow line shows the intact shear strength of cement-steel and the dashed black line is the shear strength of intact solid cement.

247

3.3. Intact Hydraulic Aperture

248

The initial hydraulic aperture of each specimen was measured with a confining pressure at ~ 3.5 MPa (effective stress of ~ 2.7 MPa) as listed in Table 2. The mean value for the initial hydraulic aperture of the cement steel samples independent of age was 6.8 ± 1.0 microns, with the error bounds representing the standard error of the full dataset. It is important to note that for each of the undeformed samples there was always fluid percolation, and none of the samples provided near zero or no flow. The solid cement samples were found to have an intact permeability of $6.50 \pm 0.36 \times 10^{-16} \text{ m}^2$ (0.65 ± 0.04 mD) equivalent to 5.38 ± 2.05 microns hydraulic aperture.

254

3.4. Effect of Shear on Hydraulic Aperture

255

The hydraulic aperture was measured for each specimen prior to and following shear failure. The changes in sample hydraulic aperture before and after shearing each sample are shown in Figure 5. It was observed that the 2 year samples showed a general increase in hydraulic aperture following shearing, whereas the 1 week and 1 month samples showed a reduction in hydraulic aperture with shearing.

258

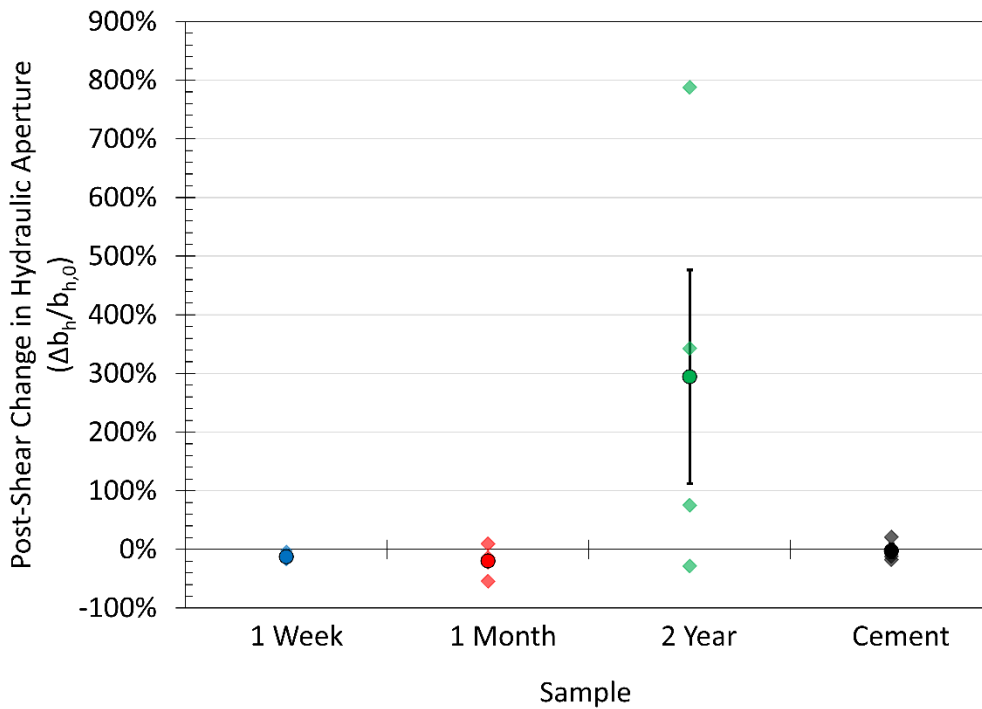
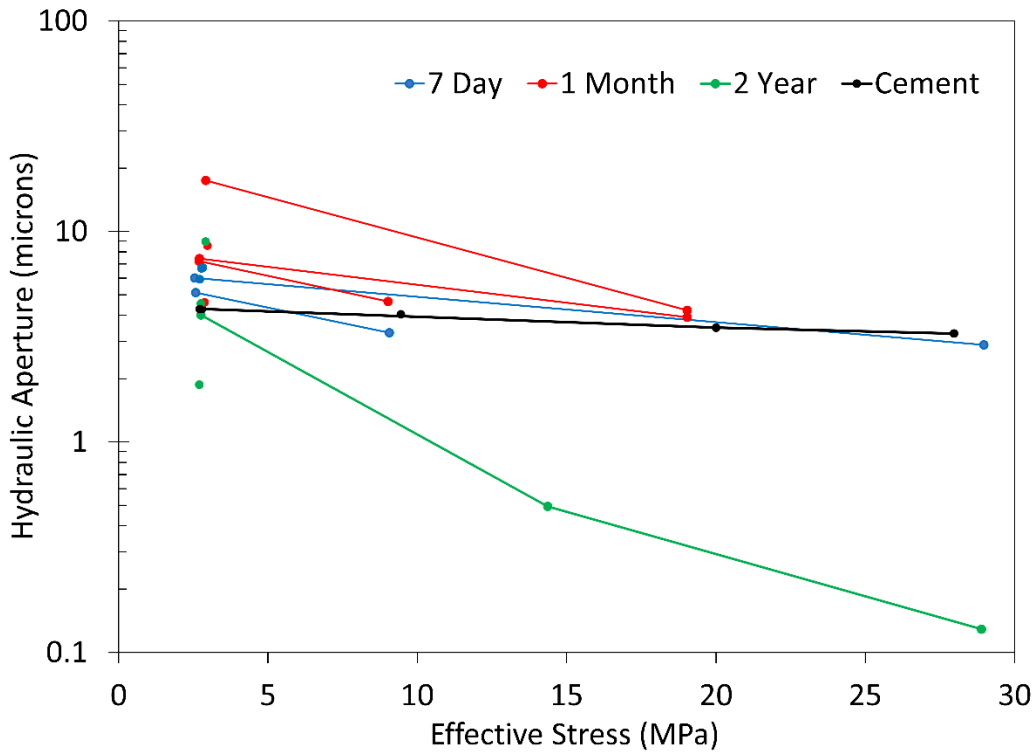


Figure 5: Relative change in sample hydraulic aperture induced by shearing normalized by the pre-shear hydraulic aperture ($b_{h,0}$). The light diamonds indicate an individual experiment measurement and the solid circle the sample set average with error bars for the standard error.

3.5. Hydraulic Aperture Effective Confining Stress Response

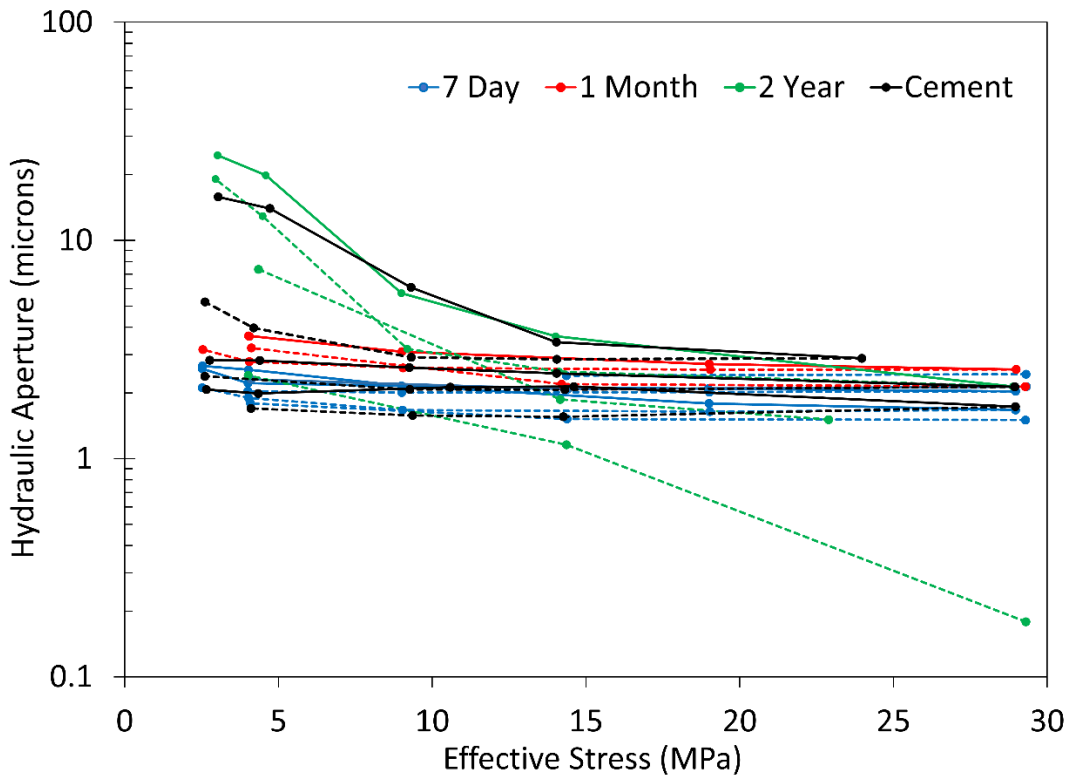
The change in hydraulic aperture with effective confining stress was explored in some of the experiments before and after shearing. The fluid flow response of the interface to changes in effective confining stress was determined by varying the confining pressure from 3.5 MPa to as much as 30 MPa while maintaining a constant displacement (no shearing). The hydraulic aperture response to changes in effective confining stress of the pre-sheared intact samples is shown in Figure 6. Trends are shown only for samples in which an elevated effective stress was applied prior to shearing. The younger 1 week and 1 month samples are less responsive to changes in effective confining stress compared to the 2 year samples. The hydraulic aperture response to loading (when available) and unloading of the post-shear samples is shown in Figure 7. The loading cycle of certain samples is abbreviated or absent depending on the final effective stress at which the sample was sheared.



273
274
275
276
277

Figure 6: Change in intact hydraulic aperture with effective confining stress prior to shear failure. Solid lines indicate the change in hydraulic aperture for each individual specimen. Unconnected data points near 2.5 MPa effective stress represent the initial intact hydraulic aperture of samples in which effective stress was not varied prior to shearing.

278



279
280
281
282

Figure 7: Change in hydraulic aperture with effective confining stress following the shear experiment without further shear displacement. Increasing confining pressure shown as solid lines and decreasing confining pressure shown as dashed lines.

3.6. Post-Experiment Surface Profilometry

Surface profilometry of the cement surface of a 1 week sample (CSS13-03) and a two year sample (CSS11-04) were recorded following shear tests to examine surface characteristics (Figure 8 and Figure 9). The root-mean-squared surface roughness (R_q) for the 1 week sample was $10.8\ \mu\text{m}$ and $4.8\ \mu\text{m}$ for the 2 year sample. The 1 week cure time sample showed numerous larger asperities as expected from a higher roughness coefficient along with a higher occurrence of deep valleys. The direction of shear was in the left to right direction, with the striations present likely caused by the grating of the two materials. In addition, no significant changes in the steel surface were observed to indicate corrosion up to the two year cure time examined.

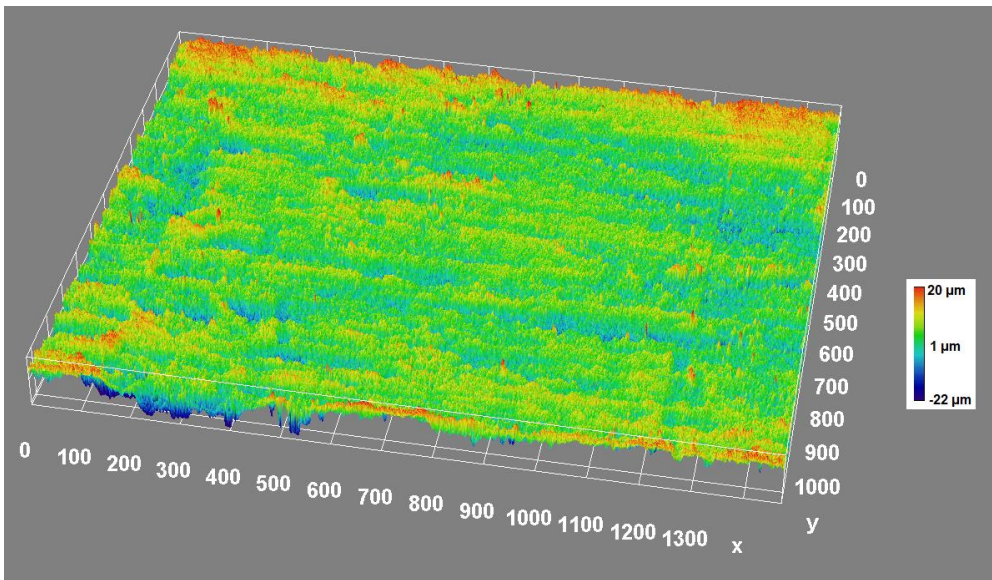


Figure 8: Surface profilometry of 1 week cement surface after shear experiments.

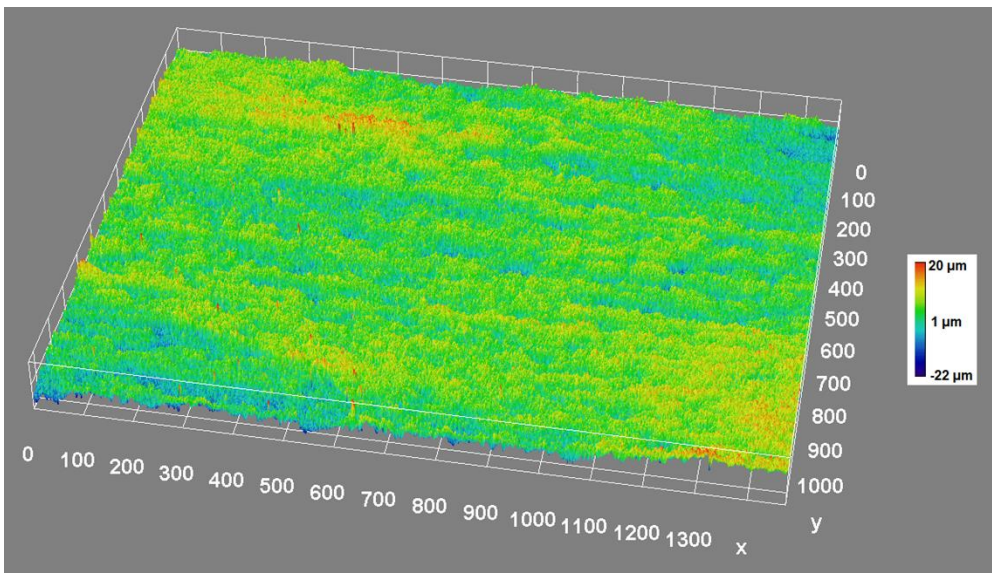


Figure 9: Surface profilometry of 2 year cement surface after shear experiments.

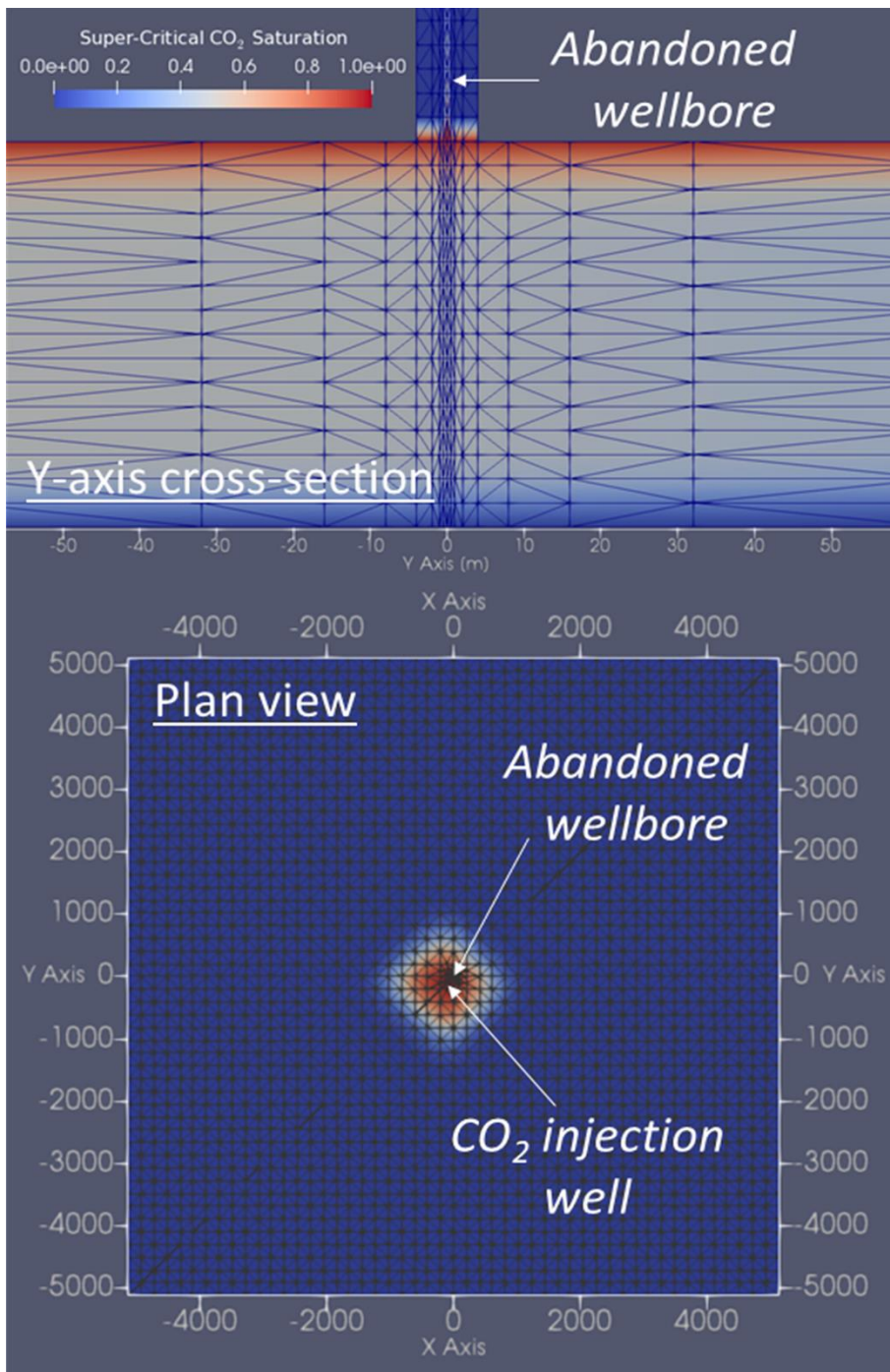
3.7. Storage site leakage simulations

CO₂ wellbore leakage simulations were performed using the measured hydraulic aperture results to determine the potential impact on long-term CO₂ injection operations (e.g., geologic carbon sequestration (GCS)). Thermal multi-phase simulations were performed with the FEHM simulator (fehm.lanl.gov), modeling supercritical CO₂ injection into a water-saturated target reservoir and subsequent leakage along a wellbore. As the CO₂ leaks up the wellbore and encounters lower pressures and temperatures, phase transitions to gas are modeled. The simulations are similar to those presented in (Harp et al., 2016). The simulation domain consisted of a 10x10 km horizontal region with a cemented wellbore in the center. The target injection reservoir was 965 m deep and 51 m thick. The initial pressure was hydrostatic based on a surface pressure of 0.2 MPa and hydraulic gradient of 9.81×10^{-3} MPa/m. The initial temperature was based on a surface temperature of 20°C and a geothermal gradient of 0.03°C/m. The lateral boundaries of the reservoir were constant pressure (Dirichlet) for both water and CO₂, allowing inflow and outflow. Intermediate reservoirs, thief zones, or aquifers were not considered here, and the CO₂ leaked directly to the atmosphere through the wellbore. The wellbore was represented with a column of 3.2 m long grid cells with 10x10 cm horizontal dimensions, resulting in an effective wellbore area of 0.01 m². The mesh spacing expanded from the 10 cm spacing at the wellbore to the 204.8 m spacing of the base mesh using octree refinement, resulting in 108,712 mesh cells. The mesh was generated using the LaGriT meshing software package (lagrit.lanl.gov).

In order to apply the measured hydraulic aperture to the wellbore permeability in the simulations, an equivalent wellbore permeability was determined by calculating the volumetric flowrate of a single planar fracture having a width equivalent to the circumference of a 15 cm (6 in) diameter well casing and aperture given by the hydraulic aperture measurements. The calculated flowrate was used in determining an equivalent permeability to apply to the 10 x 10 cm wellbore in the simulations. The mean initial hydraulic aperture (6.8 microns) and the largest aperture following shear failure (24.6 microns) were used to provide undamaged and damaged cement-steel interface leakage scenarios resulting in calculated wellbore grid cell permeabilities of 1.25×10^{-15} m² and 5.94×10^{-14} m², respectively. For simplicity, the entirety of the well bore was assumed to be cemented contrasting typical well completion designs in which only certain segments may be cemented.

We considered four scenarios, including combinations of two reservoir permeabilities of 10^{-12} and 10^{-14} m² and either a leaking injection wellbore or a leaking abandoned well 144 m from the injection well. An aerial view and

323 vertical cross-section of the simulation results for the abandoned well scenario are shown in Figure 10. The
324 abandoned well is assumed to be plugged with leakage occurring only at the external casing-cement interface.
325 The two reservoir permeabilities provide lower and higher reservoir injection pressures for the constant injection
326 simulation. CO₂ was injected at 2 kg/s (~63,000 tonnes/y) for 20 years, resulting in ~1.26 million tonnes of CO₂
327 injected. In Figure 11, we present the leakage rates for the damaged wellbore scenario (5.94×10^{-14} m²
328 permeability wellbore). The undamaged case did not produce significant leakage during the 20 years of injection.
329 The leaking injection well in the low permeability reservoir had the largest leakage rates, resulting in 47 tonnes
330 of CO₂ leaked during the 20 years. This is 3.7×10^{-3} % of the total injected CO₂, a very small percentage.



331

332

333

334

335

Figure 10: Year 1 simulation results of the abandoned well scenario in a low permeability (10^{-14} m^2) formation. The top figure is a vertical cross-section showing the carbon dioxide saturation in the storage formation and abandoned wellbore. The bottom figure shows an aerial view of the carbon dioxide saturation in the storage formation.

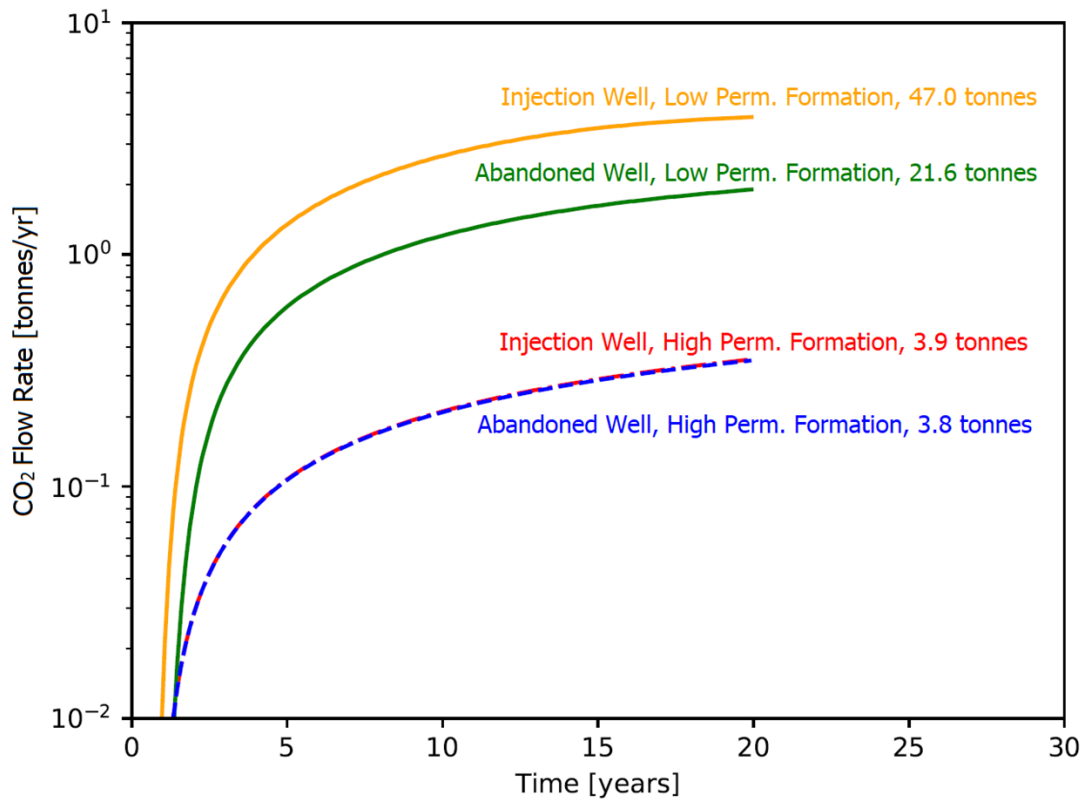


Figure 11: Well leakage rate of CO₂ to the atmosphere for a damaged injection well and nearby damaged abandoned well in a high and low permeability reservoir.

4. Discussion

4.1. Initial Shear Strength

We determined a cohesion of 1.1 ± 1.1 MPa for the intact cement-steel samples (Figure 3). The near-zero value of cohesion is consistent with experience in our laboratory where simply maneuvering samples into the testing apparatus can cause debonding unless some measure of confinement is maintained throughout (e.g., our use of a heat-shrink tubing). Very low to negligible cohesion values were also found by Lavrov et al. (2017) who found that cement-steel specimens could not be removed from a mold without breaking the bond; by Rabbat and Russell (1985) who also had difficulty handling grout-steel specimens but were able to record cohesion values ranging between 0.17 and 0.67 MPa for concrete-steel specimens; and by Kakumoto et al. (2012) who found a value of 0.79 MPa. All of these observations indicate that without significant roughening of the steel surface (e.g., by sand-blasting) cohesion of the cement-steel interface can be conservatively assigned a zero value.

By comparison, the “bond strength” results from pushout tests include a value of 0.50 ± 0.03 MPa from the work of Carter and Evans (1964); 2.2 MPa from Kakumoto et al. (2012); 8 MPa from Parceveaux and Sault (1984); 4 MPa from Hwang et al. (2018); 5.3 MPa from Silva-Neto et al. (2014); 0.4 MPa from Carpenter et al. (1992); 0.8-

0.9 MPa from Ladva et al. (2005); and 0.4 to 1.3 MPa from Lavrov et al. (2019), depending on specimen diameter. The lower values recorded in the pushout experiments are consistent with the near-zero values we measure as well as a value of 0.79 MPa determined with the triaxial system of Kakumoto et al. (2012). The high variability in push-out results is consistent with Lavrov et al.'s (2019) analysis of the limitations of the pushout test due to the uncontrolled normal stress at the cement-steel interface and emphasizes that these values should not be used to infer cement-steel bond strength.

The friction angle of the cement-steel samples was determined to be $43.4 \pm 2.0^\circ$. The pushout tests do not provide information on friction. Both Rabbat and Russell (1985) (32.6 to 35.0°) and Kakumoto et al. (2012) (28.6°) found significantly lower friction angles for concrete sliding on steel and a modified, triaxial pushout test respectively. The results indicate significant uncertainty in the friction angle.

We did not observe variability in the cohesion or friction angle of the cement-steel samples as a function of cure time. This indicates that shear strength of a well is independent of age within our observed time frame of up to 2 years.

As expected, the strength of the intact solid cement was significantly greater than the interface of the cement-steel samples with a cohesion of 6.8 ± 3.4 MPa and a friction angle $47.4 \pm 11.1^\circ$. These values show that the interface will fail before the cement at any normal effective stress. The Mohr-Coulomb failure criteria combined with the cohesion and friction angle can be used to calculate the equivalent unconfined compressive strength of the solid cement specimen at a value of 33 MPa.

4.2. Residual Shear Strength

The residual shear strength of the cement-steel interface was lower than the intact interface (Figure 4). Scatter in the results at low confining stress prevent a good measurement of the residual cohesion, but it is effectively zero. The friction angle decreased slightly from the initial shear strength value to $39.7 \pm 0.9^\circ$. A small to negligible decrease in friction angle for residual shear was previously reported for similar concrete/grout-steel samples (Rabbat and Russell, 1985). Again, we did not observe variation in the residual strength parameters as a function of cure times.

378 The friction angle of the fractured cement increased to a value of $53.0 \pm 1.8^\circ$. As shown in Figure 4, this implies
379 that a wellbore under effective shear stress $> \sim 28.4$ MPa is likely to fail through the matrix rather than along the
380 existing fracture.

381 **4.3. Hydraulic Aperture of the Cement-Steel Interface**

382 The average intact hydraulic aperture of the cement-steel samples was 6.8 ± 1.0 microns, and the permeability of
383 the solid cement was $6.50 \pm 0.36 \times 10^{-16} \text{ m}^2$ (0.65 ± 0.04 mD). In order to decouple the contribution of fluid flow
384 through the cement matrix of the cement-steel samples from that of the interface, we used the calculated flow
385 through half-circle of cement. This results in a contribution of 4.3 ± 1.6 microns to the hydraulic aperture of the
386 cement-steel interface. This value appears to be a large, however, due to the cubic-law relationship of aperture
387 to flow assumed in the parallel plate fracture flow model, this only accounts for 24.7% of flow for a 6.8 micron
388 aperture. The remaining flow results in a hydraulic aperture of 6.2 ± 1.7 microns attributed directly to the interface
389 in the samples. These flow measurements also indicate that while very low, both cement and the cement-steel
390 interface have measurable flow properties and would likely not provide a perfect seal.

391 The intact hydraulic apertures of the 2 year aged samples were smaller than the younger samples. Mineral
392 changes were also observed on the surface of the 2 year samples upon removal from the calcium hydroxide
393 storage solution. These may have affected the pore space of the cement at the steel surface, as well as additional
394 modification of the pore space in the interior of the sample. This could cause a reduction in the permeability of
395 the cement matrix and possibly the cement-steel interface.

396 The change in hydraulic aperture with shear displacement was studied in both the cement-steel interface
397 samples and the cement (Figure 5). The older 2 year samples had a significant increase in hydraulic aperture
398 following shearing; whereas the younger samples and the solid cement showed a decrease in hydraulic aperture.
399 This means that shear failure at the cement-interface in younger wells does not increase potential leakage. Wells
400 over 2 years of age are susceptible to increases of $>100x$ leakage rates following shearing. Subsequent shear
401 events at elevated effective stresses (>15 MPa) causes a reduction in hydraulic aperture to values similar or
402 lower to the intact initial sample hydraulic aperture.

403 The hydraulic aperture of a shear-damaged interface converged toward 2-3 μm hydraulic aperture as effective
404 confining stress increased in all but one 2-year old sample (Figure 7). The impact on younger interfaces was

405 modest with changes of less than 1 μm in hydraulic aperture. The 2-year old interface and the cement specimen
406 showed much stronger, but variable hydraulic aperture changes ranging up to a factor of 10. Thus leakage
407 through older shear-damaged cement-steel interfaces appears to be more sensitive to changes in confining
408 stress.

409 The cause of the variability in the hydraulic aperture response of the younger and older cure time samples has
410 not been determined. Previous work has shown that the compressive strength of cement continues to increase
411 with cure time. Samples kept in a water-rich environment will continue to gain compressive strength for at least
412 one year. In contrast, samples allowed to cure in open air environments will approach their maximum
413 compressive strength within one month albeit significantly lower than that of water—cured cement (Gonnerman
414 and Shuman, 1928; Kosmatka et al., 2002; Wood, 1992). These differences in cement compressive strength can
415 cause changes in the strength of asperities in the sheared interface, reducing the self-propping of the sheared
416 younger samples.

417 **4.4. Surface Profilometry**

418 Following experimentation it was noted that there were significant differences in the appearance of the surfaces
419 of the cement as a function of cure time. The 2 year old samples were stored in a calcium hydroxide solution,
420 which may have allowed for physical changes to occur within the cement not seen in the younger samples stored
421 in a closed container. The change in surface roughness was quantified using profilometry (Figure 8 and Figure
422 9), and the 2 year old sample ($R_q = 4.8$ microns) had a significantly smoother surface than the younger samples
423 ($R_q = 10.8$ microns). The intact and shear damaged 2 year old samples also had significantly lower hydraulic
424 apertures at high effective stresses that may have been the result of this smoother surface.

425 **4.5. Numerical Simulations**

426 The results from this experimental work were incorporated in a numerical simulation to understand what impact
427 the measured hydraulic apertures would have in terms of the total leakage from a carbon dioxide storage site.
428 The results for leakage from an injection well at a depth of 965 m indicates that even for the worst case scenario
429 (shear-damaged injection well in a low permeability reservoir), the leakage would be extremely small (3.7×10^{-3}
430 % of the injected CO_2 over a 20 year injection period). Simulations of undamaged wellbores resulted in even
431 lower leakage quantities. However, these calculations do not consider other damage mechanisms such as
432 injection-induced hydraulic failure of the cement-steel interface that could contribute to additional leakage.

5. Conclusions

In this study we performed triaxial direct shear tests to evaluate the strength of the cement-casing interface under controlled boundary conditions. Results demonstrate cohesion is negligible (1.1 ± 1.1 MPa) and does not significantly contribute to the mechanical integrity of the cement-steel system. Instead, resistance to shear damage at the cement-steel interface arises solely from friction showing that it is the normal stress at the interface that holds the casing in place. These results highlight the importance of the at present unknown stress state of cement in the wellbore environment (Welch et al., 2019). The measured friction angle of $43.4 \pm 2.0^\circ$ is relatively high compared with previous work that ranged from 28 - 35° and could still use additional work to determine the source of this variation. Experiments on the residual shear strength showed a further reduction of cohesion and a decrease of friction angle to $39.7 \pm 0.9^\circ$. We did not observe variability in strength properties as a function of cure time ranging from 1 week to 2 years.

We characterized the permeability of the cement-steel interface in terms of hydraulic aperture using a cubic-law relationship to permeability. The hydraulic aperture of the intact cement-steel interface was 6.2 ± 1.7 microns after correcting for flow contributions for the matrix. This value is equivalent to a permeability of 4 mD for a 2.5-cm thick cement surrounding a 15 cm (6 inch) diameter pipe. Shearing of the interface did not increase the permeability of 1 week and 1 month cements, but did increase the hydraulic aperture up to 24.6 microns for a 2 year aged sample.

With respect to well leakage, simulation of leakage from an injection and an abandoned well during a 20-year injection using these measurements indicate that the cement-casing interface is not a significant leakage pathway in its intact or damaged state. Thus, our results indicate that shear-driven failure scenarios for this interface are not a significant risk to CO_2 storage security. However, the very low cohesion of the cement-steel interface indicates that hydraulic failure of the interface could occur where fluid pressure exceeds the normal stress at the interface. Current lack of understanding of the normal stress at this interface is a key unknown in risk studies of wellbore integrity.

6. Data Availability

Datasets related to this article can be found at <http://dx.doi.org/10.17632/hbwgp2jm6d.1>, an open-source online data repository hosted at Mendeley Data (N J Welch et al., 2019).

7. Acknowledgements

We wish to thank the Department of Energy—Fossil Energy program for support through FWP LANL FE-890-18-FY19 and for program guidance from Joshua Hull and Tracy Rodosta. Released under LA-UR-19-31213.

8. References

- Benson, S., Cook, P., 2005. Chapter 4 - Underground Geological Storage, in: Carbon Dioxide Capture and Storage. Cambridge University Press, p. 208.
- Bois, A.R., Gamier, A., Rodot, F., Saint-Marc, J., Aimard, N., 2011. How to prevent loss of zonal isolation through a comprehensive analysis of microannulus formation. SPE Drill. Complet. <https://doi.org/10.2118/124719-PA>
- Carey, J.W., 2013. Geochemistry of Wellbore Integrity in CO₂ Sequestration: Portland Cement-Steel-Brine-CO₂ Interactions. Rev. Mineral. Geochemistry. <https://doi.org/10.2138/rmg.2013.77.15>
- Carey, J.W., Lei, Z., Rougier, E., Mori, H., Viswanathan, H., 2015. Fracture-permeability behavior of shale. J. Unconv. Oil Gas Resour. <https://doi.org/10.1016/j.juogr.2015.04.003>
- Carey, J.W., Wigand, M., Chipera, S.J., WoldeGabriel, G., Pawar, R., Lichtner, P.C., Wehner, S.C., Raines, M.A., Guthrie, G.D., 2007. Analysis and performance of oil well cement with 30 years of CO₂ exposure from the SACROC Unit, West Texas, USA. Int. J. Greenh. Gas Control. [https://doi.org/10.1016/S1750-5836\(06\)00004-1](https://doi.org/10.1016/S1750-5836(06)00004-1)
- Carpenter, R.B., Brady, J.L., Blount, C.G., 1992. Effects of temperature and cement admixes on bond strength. JPT J. Pet. Technol. <https://doi.org/https://doi.org/10.2118/22063-PA>
- Carroll, S., Carey, J.W., Dzombak, D., Huerta, N.J., Li, L., Richard, T., Um, W., Walsh, S.D.C., Zhang, L., 2016. Role of chemistry, mechanics, and transport on well integrity in CO₂ storage environments. Int. J. Greenh. Gas Control 49, 149–160.

482 Carter, G., Evans, G.W., 1964. A Study of Cement-Pipe Bonding. *J. Pet. Technol.* <https://doi.org/10.2118/764->
483 PA

484 Crow, W., Carey, J.W., Gasda, S., Brian Williams, D., Celia, M., 2010. Wellbore integrity analysis of a natural
485 CO₂ producer. *Int. J. Greenh. Gas Control* 4, 186–197. <https://doi.org/10.1016/J.IJGGC.2009.10.010>

486 Dahi Taleghani, A., Wang, W., 2016. Emergence of Delamination Fractures Around the Casing and Its Stability.
487 *J. Energy Resour. Technol.* 139, 12904–12911.

488 Dusseault, M.B., Gray, M.N., Nawrocki, P. a, 2000. Why Oilwells Leak : Cement Behavior and Long-Term
489 Consequences. *SPE Int. Oil Gas Conf. Exhib. SPE 64733.* <https://doi.org/10.2118/64733-MS>

490 Evans, G.W., Carter, L.G., 1962. Bonding studies of cementing compositions to pipe and formations, in:
491 *Southwestern District, API Division of Production.*

492 Feng, Y., Li, X., Gray, K.E., 2017. Development of a 3D numerical model for quantifying fluid-driven interface
493 debonding of an injector well. *Int. J. Greenh. Gas Control* 62, 76–90.
494 <https://doi.org/10.1016/J.IJGGC.2017.04.008>

495 Frash, L.P., Carey, J.W., 2018. Engineering Prediction of Axial Wellbore Shear Failure Caused by Reservoir
496 Uplift and Subsidence. *SPE J.* 23, 1039–1066. <https://doi.org/10.2118/189981-PA>

497 Frash, L.P., Carey, J.W., Ickes, T., Viswanathan, H.S., 2017. Caprock integrity susceptibility to permeable
498 fracture creation. *Int. J. Greenh. Gas Control.* <https://doi.org/10.1016/j.ijggc.2017.06.010>

499 Frash, L.P., Carey, J.W., Lei, Z., Rougier, E., Ickes, T., Viswanathan, H.S., 2016. High-stress triaxial direct-shear
500 fracturing of Utica shale and in situ X-ray microtomography with permeability measurement. *J. Geophys.*
501 *Res. Solid Earth.* <https://doi.org/10.1002/2016JB012850>

502 Genedy, M., Stormont, J., Matteo, E., Taha, M.R., 2014. Examining epoxy-based nanocomposites in wellbore
503 seal repair for effective CO₂ sequestration, in: *Energy Procedia.*
504 <https://doi.org/10.1016/j.egypro.2014.11.612>

505 Gonnerman, H.F., Shuman, E.C., 1928. Compression, Flexure and Tension Tests of Plain Concrete. *Rep. Dir.*
506 *Res.* 149–163.

507 Harp, D.R., Pawar, R., Carey, J.W., Gable, C.W., 2016. Reduced order models of transient CO₂ and brine
508 leakage along abandoned wellbores from geologic carbon sequestration reservoirs. *Int. J. Greenh. Gas*
509 *Control*. <https://doi.org/10.1016/j.ijggc.2015.12.001>

510 Hwang, J., Ahmed, R., Tale, S., Shah, S., 2018. Shear bond strength of oil well cement in carbonic acid
511 environment. *J. CO₂ Util.* <https://doi.org/10.1016/j.jcou.2018.07.001>

512 Kakumoto, M., Yoneda, J., Tenma, N., Miyazaki, K., Aoki, K., Itoi, R., 2012. Frictional strength between casing
513 and cement under confining pressure, in: *Proceedings of the International Offshore and Polar Engineering*
514 *Conference*.

515 Kosmatka, S.H., Kerkhoff, B., Panarese, W.C., 2002. *Design and control of concrete mixtures*, 14th ed. Portland
516 Cement Association Skokie, IL.

517 Ladva, H.K.J., Craster, B., Jones, T.G.J., Goldsmith, G., Scott, D., 2005. The cement-to-formation interface in
518 zonal isolation. *SPE Drill. Complet.* <https://doi.org/10.2118/88016-PA>

519 Lavrov, A., Bhuiyan, M., Stroisz, A., 2019. Push-out test: Why bother? *J. Pet. Sci. Eng.* 172, 297–302.
520 <https://doi.org/10.1016/j.petrol.2018.09.067>

521 Lavrov, A., Gawel, K., Stroisz, A., Torsæter, M., Bakheim, S., 2017. Failure modes in three-point bending tests
522 of cement-steel, cement-cement and cement-sandstone bi-material beams. *Constr. Build. Mater.*
523 <https://doi.org/10.1016/j.conbuildmat.2017.07.017>

524 Lecampion, B., Bungler, A., Kear, J., Quesada, D., 2013. Interface debonding driven by fluid injection in a cased
525 and cemented wellbore: Modeling and experiments. *Int. J. Greenh. Gas Control* 18, 208–223.
526 <https://doi.org/10.1016/J.IJGGC.2013.07.012>

527 Liu, X., Nair, S.D., Cowan, M., Van Oort, E., 2015. A novel method to evaluate cement-shale bond strength, in:
528 *Proceedings - SPE International Symposium on Oilfield Chemistry*.

529 Parcevaux, P.A., Sault, P.H., 1984. Cement shrinkage and elasticity: a new approach for a good zonal isolation,
530 in: *SPE Annual Technical Conference and Exhibition*. Society of Petroleum Engineers.

531 Rabbat, B.G., Russell, H.G., 1985. Friction Coefficient of Steel on Concrete or Grout. *J. Struct. Eng.*

532 [https://doi.org/10.1061/\(ASCE\)0733-9445\(1985\)111:3\(505\)](https://doi.org/10.1061/(ASCE)0733-9445(1985)111:3(505))

533 Silva Neto, J.F., Silva, E.P., Gomes, K.C., Torres, S.M., de Barros, S., 2014. Numerical and experimental
534 investigation of shear strength between the steel tube and cement paste in petroleum wells. *Appl. Adhes.*
535 *Sci.* <https://doi.org/10.1186/2196-4351-2-4>

536 U.S. E.P.A., 2012. Underground Injection Control (UIC) Program Class VI Well Construction Guidance.

537 Watson, T.L., Bachu, S., 2009. Evaluation of the Potential for Gas and CO₂ Leakage Along Wellbores. *SPE Drill.*
538 *Compleat.* <https://doi.org/10.2118/106817-PA>

539 Welch, N. J., Frash, L.P., Carey, J.W., 2019. Effective cement stress in well completions: An important unknown,
540 in: 53rd U.S. Rock Mechanics/Geomechanics Symposium.

541 Welch, N J, Frash, L.P., Harp, D.H., Carey, J.W., 2019. Data for: Cement-Steel Shear Strength and Permeability
542 Measurements [WWW Document]. Mendeley Data.
543 <https://doi.org/http://dx.doi.org/10.17632/hbwgp2jm6d.1>

544 Wood, S.L., 1992. Evaluation of the Long-Term Properties of Concrete. *Portl. Cem. Assoc.* 99.
545 <https://doi.org/10.14359/1201>

546 Zhang, M., Bachu, S., 2011. Review of integrity of existing wells in relation to CO₂ geological storage: What do
547 we know? *Int. J. Greenh. Gas Control* 5, 826–840. <https://doi.org/10.1016/J.IJGGC.2010.11.006>

548 Zimmerman, R.W., Bodvarsson, G.S., 1996. Hydraulic conductivity of rock fractures. *Transp. Porous Media.*
549 <https://doi.org/10.1007/BF00145263>

550